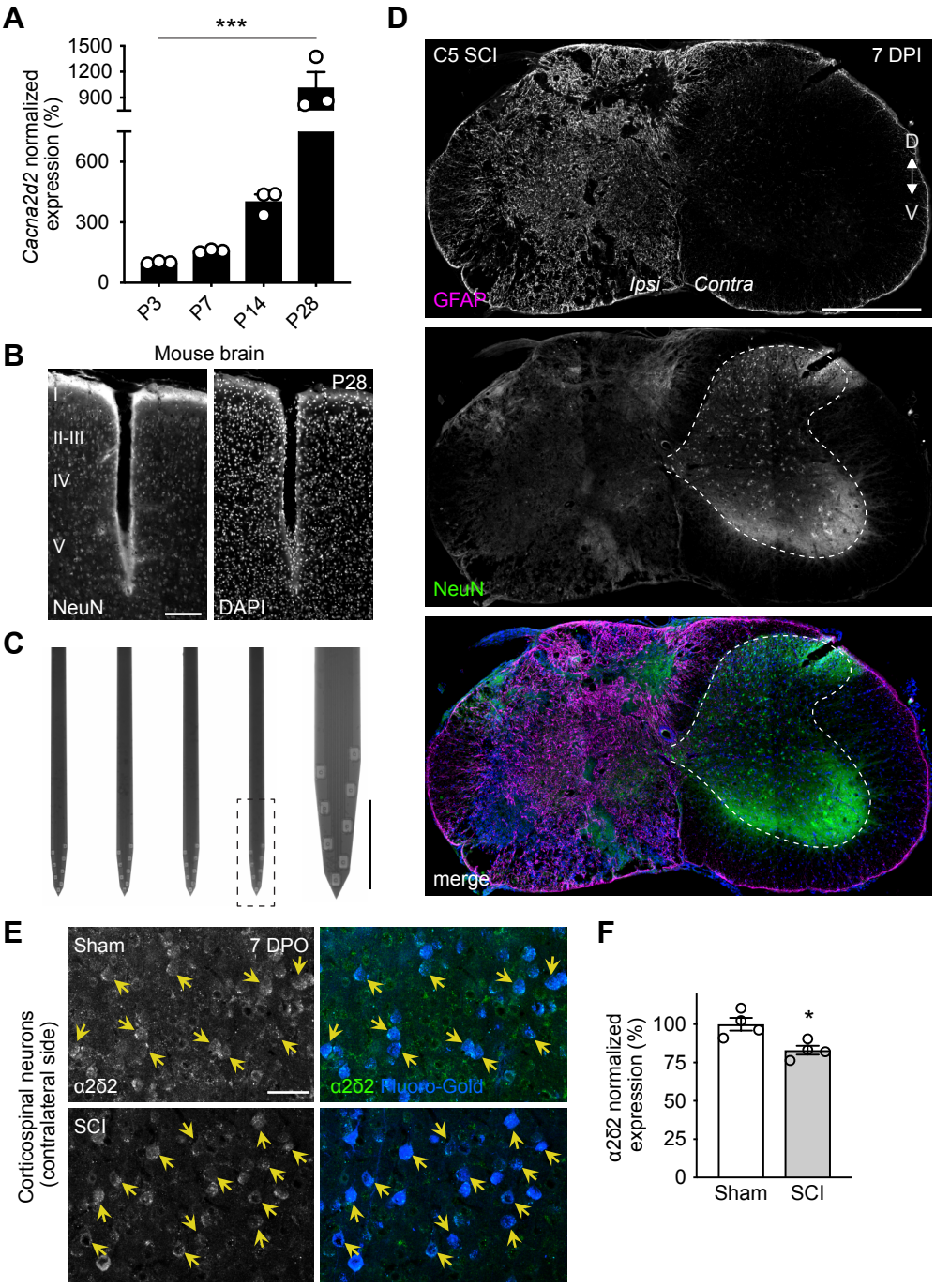

Supplemental Figure 1. Developmental changes in *Cacna2d2* expression and experimental models of *in vivo* recording and cervical SCI. (**A**) *Cacna2d2* expression within the sensory-motor cortex was measured by qRT-PCR at different stages of brain development. Mean and SEM (linear trend test after log-2 transformation ***p<0.001; triplicate experiments). (**B**) Sagittal section of the mouse brain immunostained with NeuN antibody. Roman numerals indicate cortical layers. DAPI stained nuclei. The position of the electrode shank is clearly visible. Scale bar, 200 µm. (**C**) Electrode array (Buzsaki 32). Scale bar, 100 µm. (**D**) Coronal section of the injured spinal cord stained using GFAP and NeuN antibodies (DPI: days post injury, D: dorsal, V: ventral). The white dashed line indicates the grey matter. DAPI stained nuclei. Scale bar, 500 µm. (**E**) Representative fluorescence images of contralateral retrogradely labeled corticospinal neurons (yellow arrows) 7 days after C5 SCI (DPO, days post operation). Sagittal sections of the mouse brain (left hemisphere) were immunostained with α2δ2 antibody. Scale bar, 50 µm. (**F**) Quantification of (E). Mean and SEM (unpaired two-tailed Student's t test *p<0.05; sham n=4 and SCI n=4 mice, 166-228 neurons per condition).

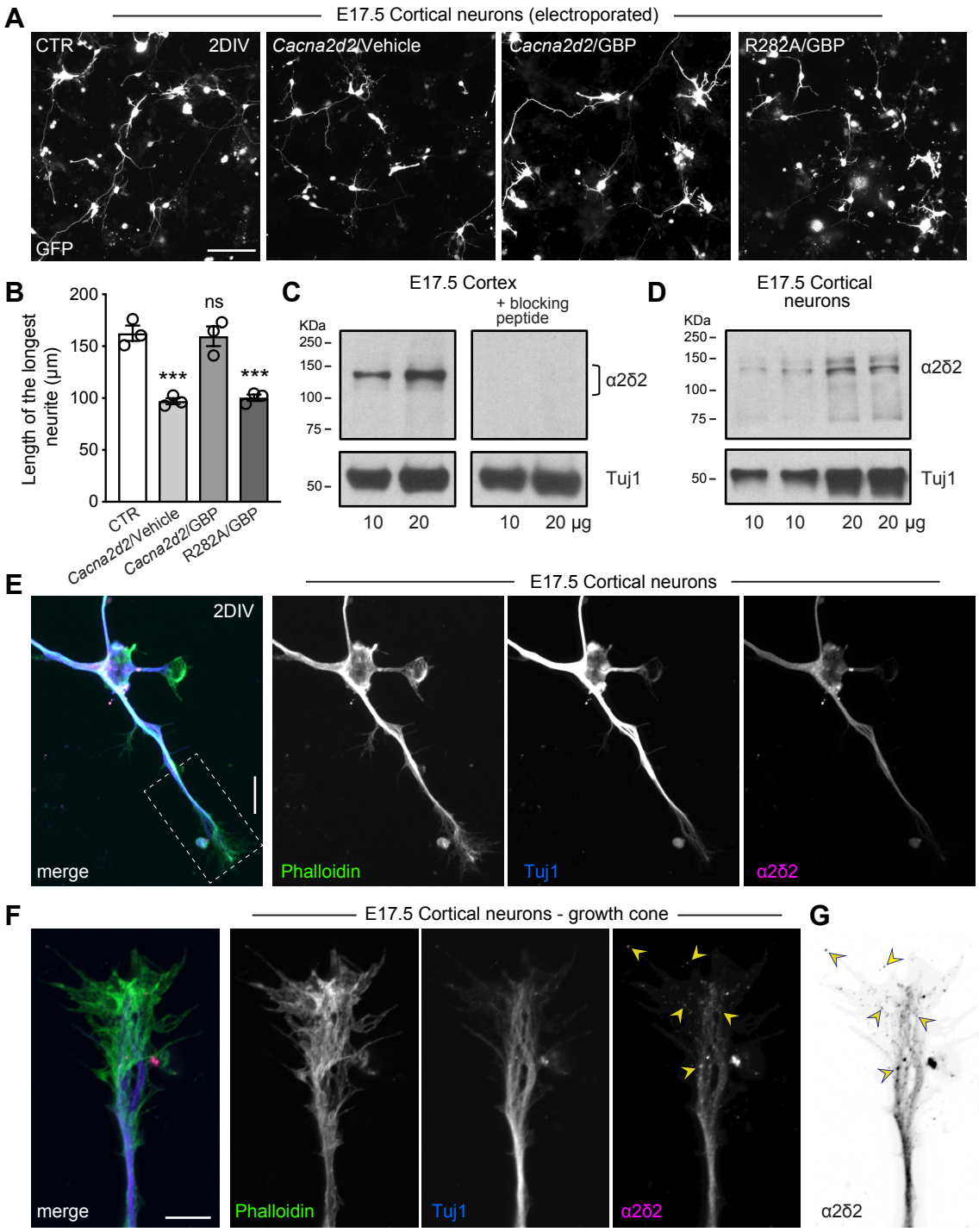

Supplemental Figure 2. Mouse embryonic cortical neurons express α2δ2. (**A**) Representative fluorescence images of mouse E17.5 cortical neurons cultured for 48 hours after electroporation with GFP plus either CTR, *Cacna2d2* or *Cacna2d2*/R282A expressing plasmids in the presence of vehicle (0.9% Saline) or 250 µM GBP (DIV: day in vitro). Scale bar, 100 µm. (**B**) Quantification of (A). Mean and SEM (one-way ANOVA followed by Dunnett posttest ***p<0.001 ns, not significant; triplicate experiments; 143-164 neurons per condition). (**C**) Immunoblot shows α2δ2 expression in E17.5 mouse sensory-motor cortex. To determine antibody specificity, the α2δ2 antibody was pre-incubated with its immunizing peptide (right panel). Tuj1 is used as loading control. (**D**) Immunoblot shows α2δ2 expression in dissociated E17.5 mouse cortical neurons (n=2 independent biological replicates). Tuj1 is used as loading control. (**E**) Mouse E17.5 cortical neurons were cultured for two days and stained with Phalloidin, Tuj1 and α2δ2 antibodies. Scale bar, 10 µm. (**F**) Fluorescence images of the growth cone shown in (E) (dashed box). Arrow heads indicate α2δ2 punctate staining. Scale bar, 5 µm. (**G**) α2δ2 fluorescence image in (F) was inverted and processed using Golay filter.

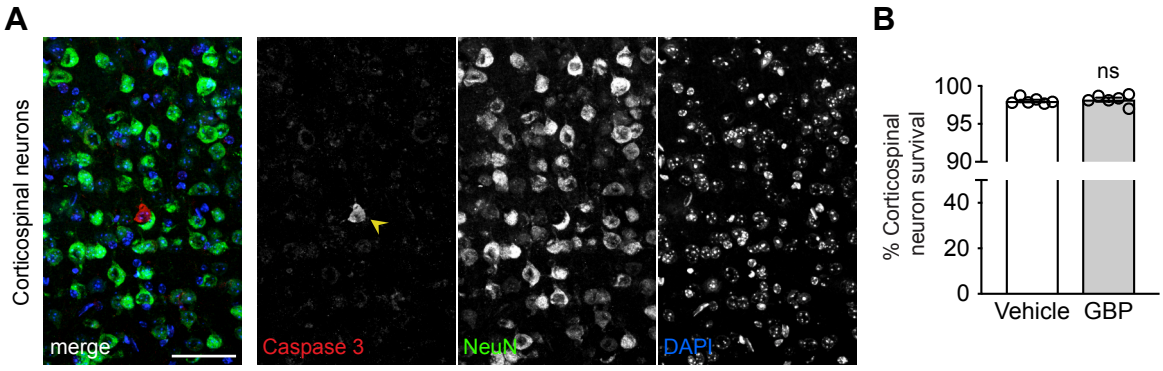

Supplemental Figure 3. α2δ2 pharmacological blockade does not affect cortical survival after PTX in adulthood. (**A**) Representative fluorescence images of corticospinal neurons 4 weeks after PTX. Sagittal sections of the mouse brain (right hemisphere) were immunostained with activated Caspase 3 and NeuN antibodies. The arrow indicates a corticospinal neuron with activated Caspase 3. DAPI stained nuclei. Scale bar, 50 µm. (**B**) Quantification of (A). Mean and SEM (unpaired two-tailed Student's t test ns, not significant; vehicle n=6 and GBP n=6; 1914-2012 neurons per condition).

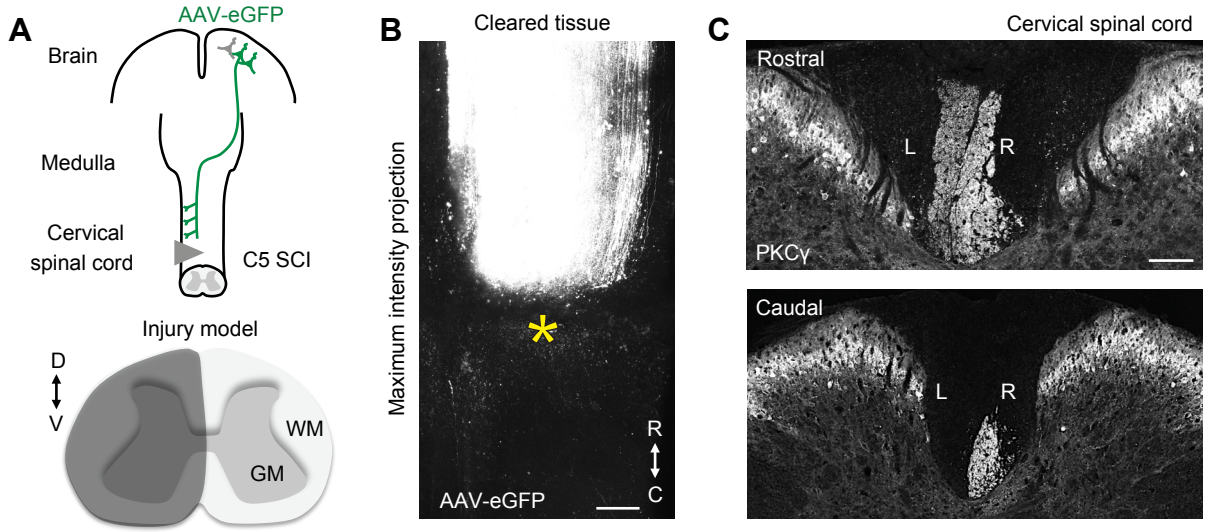

Supplemental Figure 4. A C5 SCI model that completely severs corticospinal axons. (**A**) Schematic of corticospinal tracing and C5 SCI (D: dorsal, V: ventral, GM: grey matter, WM: white matter). (**B**) Automated tile scanning of the cleared and unsectioned adult spinal cord 6 weeks after cervical SCI. Corticospinal axons were labeled by injecting AAV-eGFP into the right sensory-motor cortex (R: rostral, C: caudal). Asterisk indicates the lesion epicenter. Scale bar, 200 μm. (**C**) Coronal sections of the spinal cord rostral and caudal to the lesion were stained using PKCγ antibody to confirm completeness of lesion (L: left, R: right; n=12 mice). Scale bar, 100 μm.

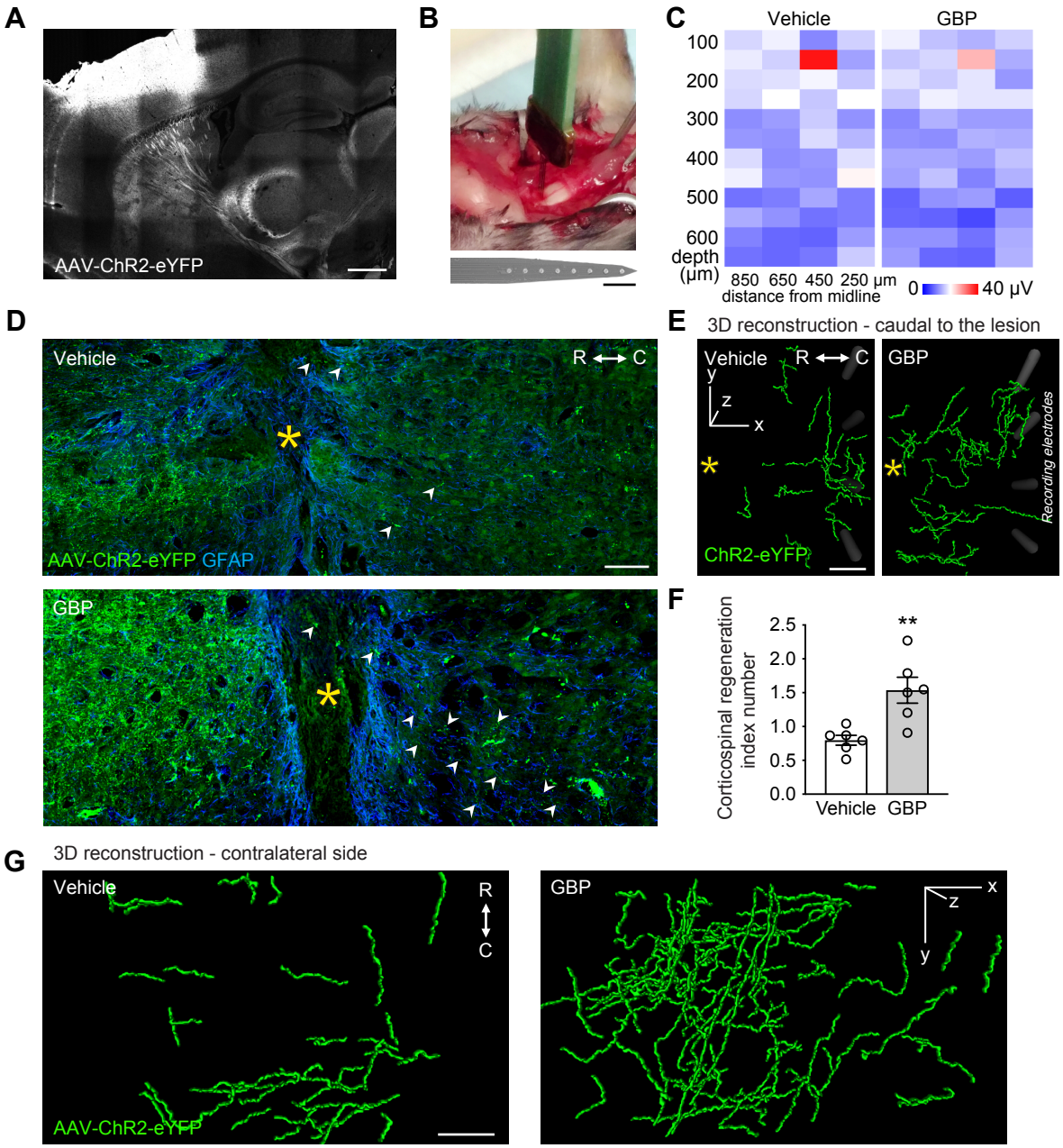

Supplemental Figure 5. Dissecting corticospinal structural and functional changes after C5 SCI. (**A**) Sagittal section of the mouse brain one month after AAV-ChR2-eYFP injection into the right sensory-motor cortex (automated tile scanning). Scale bar, 1 mm. (**B**) Photographs showing an *in vivo* recording session and one of a 4 shank electrode array (A4x8-5mm-50-200-177-A32). Scale bar, 100 μm. (**C**) Heatmap (z-transformed, blue to red) to visualize changes in corticospinal connectivity caudal to the injury site. Each box represents average data from a single electrode, each column a single electrode shank (vehicle n=6 and GBP n=6 mice). (**D**) Representative images of sagittal sections 4 months after SCI. AAV-ChR2-eYFP was injected into the right sensory-motor cortex to label and optically stimulate corticospinal axons. Sections were stained with GFP and GFAP antibodies (R: rostral, C: caudal). Asterisk indicates the lesion epicenter and arrow heads indicate regenerating corticospinal axons. Scale bar, 100 μm. (**E**) Semi-automatic 3D skeletonization of regenerating corticospinal axons (caudal to the lesion site) in the unsectioned spinal cord 4 months after SCI (R: rostral, C: caudal). Asterisk indicates the lesion site. Grey bars represent the 4 shanks of the multichannel electrode array. Scale bar, 100 μm. (**F**) Quantification of (D). Mean and SEM (unpaired two-tailed Student's t test **p<0.01; vehicle n=6 and GBP n=6 mice). (**G**) Semi-automatic 3D skeletonization of regenerating axons in the contralateral side (rostral to the injury site) of the unsectioned spinal cord 4 months after SCI (vehicle n=6 and GBP n=6 mice). Scale bar, 100 μm.

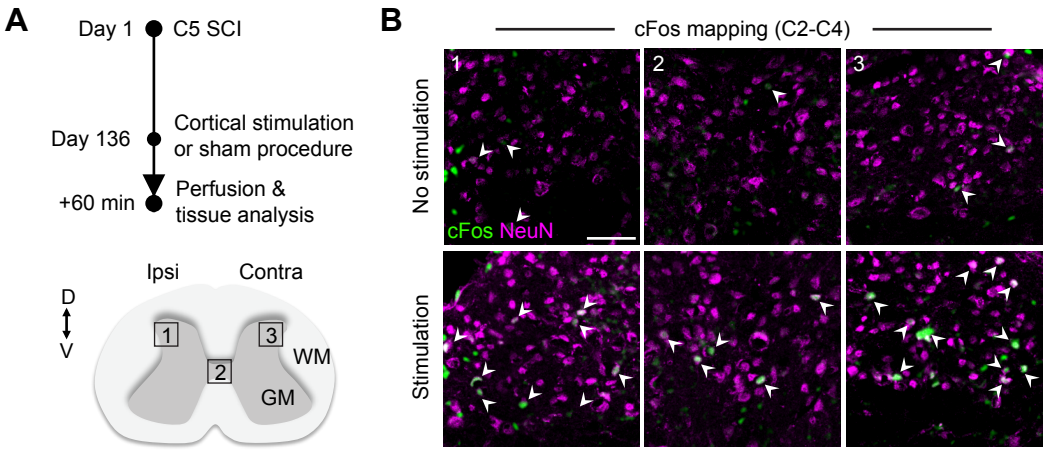

Supplemental Figure 6. cFos activity mapping of the injured spinal cord. (**A**) Experimental scheme of (B). (**B**) Coronal sections of the spinal cord rostral to the lesion were stained using cFos and NeuN antibodies and imaged using automatic tile scanning. cFos images were then processed through a 7x7 pixel Gaussian filtering protocol. The arrow heads indicate cFos/NeuN positive neurons. Scale bar, 50 µm.

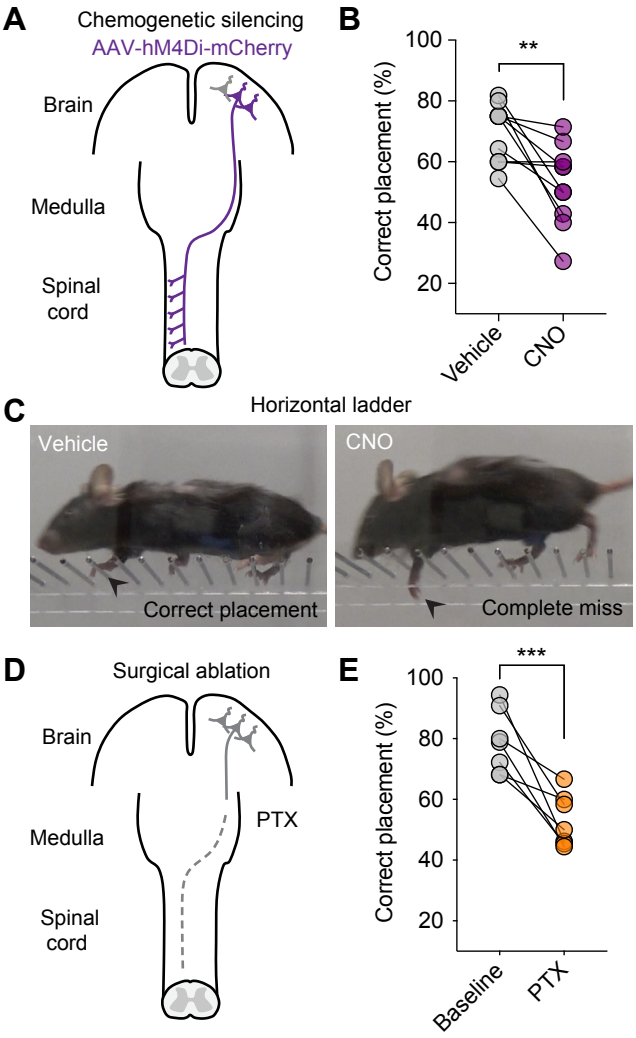

Supplemental Figure 7. Chemogenetic silencing and surgical ablation of the corticospinal pathway impairs forelimb skilled walking in mice. (**A**) Schematic of chemogenetic experiment in (B). (**B**) Transient activation of hM4Di in corticospinal neurons impaired forelimb skilled walking. Scatter plot (paired two-tailed Student's t-test **p<0.01; n=10 mice). (**C**) Representative images of correct placement and complete miss. (**D**) Schematic of the surgical ablation experiment in (E). (**E**) Forelimb skilled walking is impaired 7 days after unilateral PTX. Scatter plot (paired two-tailed Student's t-test ***p<0.001; n=7 mice).

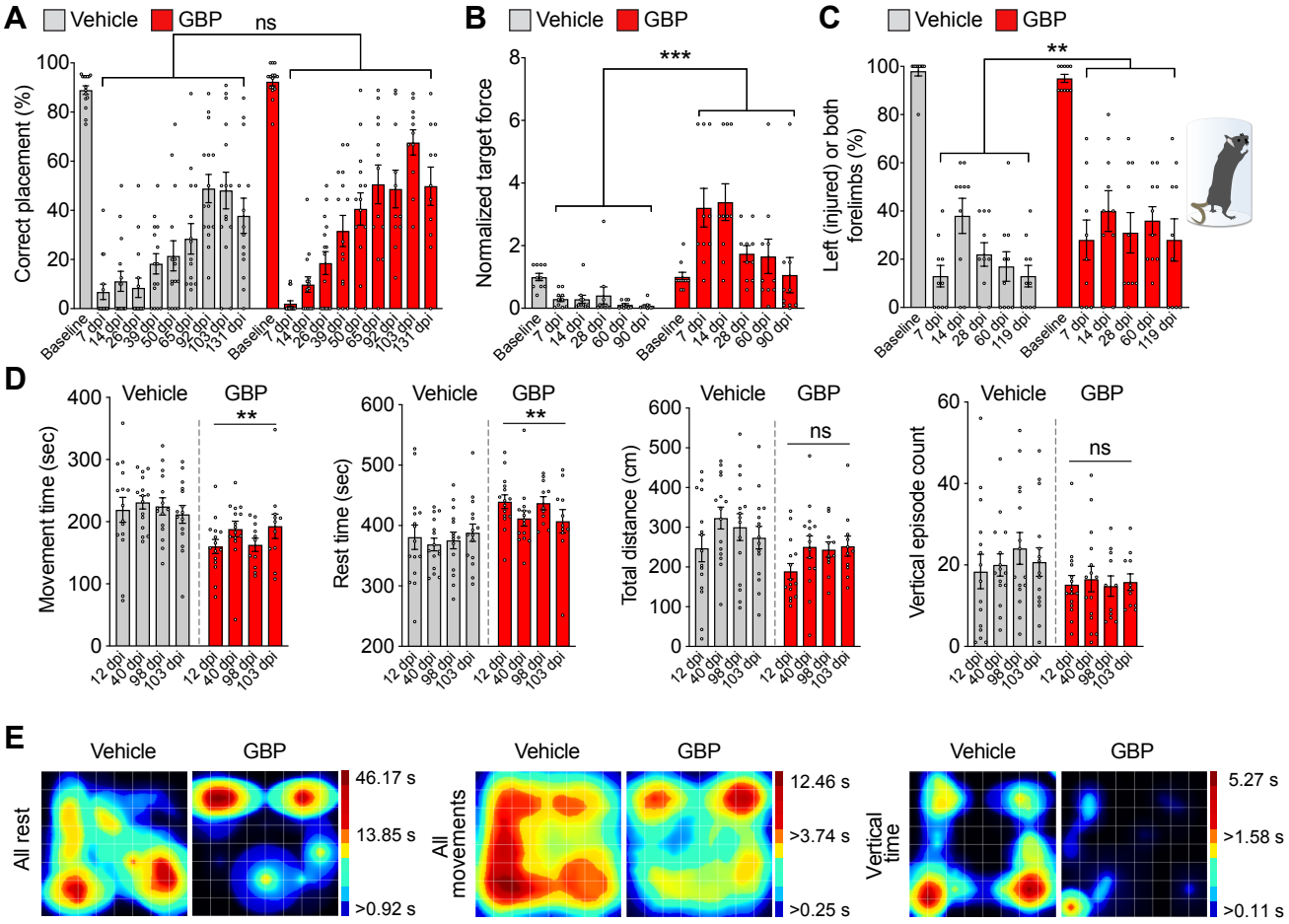

Supplemental Figure 8. Assessing behavioral changes and recovery in mice after cervical SCI.
(**A**) Recovery of hindlimb skilled locomotor function was measured using the horizontal ladder rung-walking test. Mean and SEM (mixed model with repeated measures using compound symmetry covariance structure and controlled on baseline values ns, not significant; vehicle n=15 and GBP n=15 mice). (**B**) The mechanical threshold of the plantar surface of the mouse hindpaw (left side) was measured using the Von Frey test. Mean and SEM (mixed model with repeated measures using compound symmetry covariance structure and controlled on baseline values ***p<0.01; vehicle n=10 and GBP n=10 mice). (**C**) Recovery of forelimb symmetry in rearing was measured using the cylinder test. Mean and SEM (mixed model with repeated measures using compound symmetry covariance structure and controlled on baseline values **p<0.01; vehicle n=10 and GBP n=10 mice). (**D**) Activity box. Mean and SEM (**p<0.01; ns: not significant; dpi: days post injury; vehicle n=15 and GBP n=15 mice). (**E**) Representative images of (D) at 103 days after C5 SCI.